RESEARCH ARTICLE | OCTOBER 18 2022

Joint experimental and theoretical study on electron scattering from titanium tetrachloride ($TiCl_4$) molecule

Natalia Tańska; Pedro A. S. Randi ; Sylwia Stefanowska-Tur; Giseli M. Moreira ; Elżbieta Ptasińska-Denga; Márcio H. F. Bettega ; Czesław Szmytkowski ; Paweł Możejko

J. Chem. Phys. 157, 154301 (2022)
https://doi.org/10.1063/5.0116713

The Journal of Chemical Physics ARTICLE scitation.org/journal/jcp

Joint experimental and theoretical study on electron scattering from titanium tetrachloride ($TiCl_4$) molecule

Cite as: J. Chem. Phys. 157, 154301 (2022); doi: 10.1063/5.0116713
Submitted: 29 July 2022 • Accepted: 22 September 2022 •
Published Online: 18 October 2022

Natalia Tańska,[1,a] Pedro A. S. Randi,[2,b] Sylwia Stefanowska-Tur,[1,c] Giseli M. Moreira,[2,d] Elżbieta Ptasińska-Denga,[1,e] Márcio H. F. Bettega,[2,f] Czesław Szmytkowski,[1,g] and Paweł Możejko[1,h]

AFFILIATIONS

[1] Institute of Physics and Applied Computer Science, Faculty of Applied Physics and Mathematics, Gdańsk University of Technology, ul. Gabriela Narutowicza 11/12, 80-233 Gdańsk, Poland
[2] Departamento de Física, Universidade Federal do Paraná, Caixa Postal 19044, 81531-980 Curitiba, Paraná, Brazil

[a] natalia.tanska@pg.edu.pl
[b] pasr@fisica.ufpr.br
[c] sylstefa1@student.pg.edu.pl
[d] gmm08@fisica.ufpr.br
[e] elzdenga@pg.edu.pl
[f] bettega@fisica.ufpr.br
[g] czsz@mif.pg.gda.pl
[h] **Author to whom correspondence should be addressed:** paw@pg.edu.pl

ABSTRACT

Absolute *grand*-total cross section for electron scattering from titanium tetrachloride, $TiCl_4$, molecule was measured at electron-impact energies ranging from 0.3 to 300 eV, in the linear electron-transmission experiment. The elastic integral, differential, momentum transfer, and total ionization cross sections for $TiCl_4$ molecule were also calculated for low and intermediate collisional energies at the level of various theories. The low-energy elastic integral, differential, and momentum transfer cross sections were calculated with the Schwinger multichannel method implemented with pseudopotentials, in the static-exchange and static-exchange plus polarization levels of approximation, for energies up to 30 eV. The integral cross section calculated for low-energy electron scattering with the R-matrix method within the static-exchange and static-exchange plus polarization approximations for energies up to 15 eV are also reported. By the inspection of the cross sections, the presence of resonances is discussed. In particular, the calculated integral cross sections and the measured total cross section display a minimum at around 1 eV, which is consistent with the presence of a Ramsauer–Townsend minimum and a sharp increase at low energies, which is consistent with the presence of a virtual state. Additionally, interactions in elastic and ionization channels for intermediate collision energies were investigated with the additivity rule and the binary-encounter-Bethe methods.

I. INTRODUCTION

Electron driven collisional processes in complex environments are crucial in many chemical, astrochemical, astrobiological, and technological processes.[1] Comprehensive knowledge about electron interaction with molecules is important for a detailed description of the plasma assisted chemical vapor deposition (PA-CVD) and the molecular precursor fragmentation processes in focused electron beam induced deposition (FEBID) methods. Among the complex precursors used in these thin nanometric film deposition techniques, one of the simplest is titanium tetrachloride molecule, $TiCl_4$ (Fig. 1).[2–5] Hence, detailed information concerning electron–$TiCl_4$ collisions, including cross section data for different scattering channels and also total cross section, in a wide electron energy range, is strongly required.

There is not much research available in the literature on electron scattering from titanium tetrachloride molecules. Moreover, these studies are not too comprehensive and are limited to a few

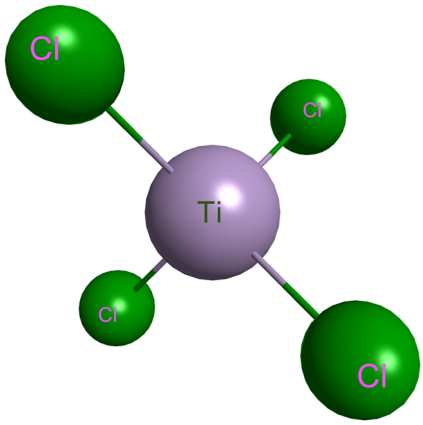

FIG. 1. Chemical structure of the $TiCl_4$ (generated with MacMolPlt[19]).

major scattering channels, such as the dissociation, ionization, and elastic channels. To date, experimental works on electron–$TiCl_4$ collisions focused mainly on the formation of positive and negative ions. The molecular structure of $TiCl_4$ has been determined by the gas electron diffraction method.[6–8] Fractional relative abundance of ions as well as appearance potentials have been studied with time-of-flight and double focusing mass spectrometers.[9] Negative ions formation due to low-energy (1–8 eV) electron interaction with $TiCl_4$ molecules has also been experimentally studied by Bennett *et al.*[10] Mathur *et al.*[11] studied negative ion formation from $TiCl_4$ in collisions with Cs atoms. Photoelectron spectra of $TiCl_4$ have been measured by Egdell and Orchard.[12] Absolute total and partial electron-impact ionization cross sections have been measured by Basner *et al.* with the time-of-flight mass spectrometer[13] for energies ranging from the ionization threshold up to 500 eV. Dissociative electron attachment study of titanium tetrachloride in the incident electron energy ranging from 0 to 18 eV has been performed with a trochoidal electron spectrometer and quadruple mass spectrometer.[14] The resonant character of electron driven processes in $TiCl_4$ has been observed and confirmed in the transmission electron experiment for impact electron energies between 0 and 10 eV.[15] So far, no measured absolute total cross section for electron scattering from $TiCl_4$ molecules has been reported. Only a relative total cross section, obtained in the energy range from 2.5 to 9 eV, evaluated from the derivative electron transmission spectrum, has been announced.[15]

To our knowledge, the only theoretical studies available reported the elastic cross section obtained using the multiple-scattering Xα method (MS Xα)[15] and the elastic integral, differential, and momentum transfer cross sections derived with the Schwinger multichannel method in the static-exchange approximation.[16] The latter studies have has also reported the total ionization cross section calculations with the binary-encounter-Bethe method, in which target properties have been obtained using the Hartree–Fock method with a 3-21G(3*d*) basis set.[16] Total ionization cross section for impact-electron energies ranging from the ionization threshold to 500 eV has been also calculated with the semiempirical Deutsch–Märk (DM) method.[17] The ionization peak cross section value has been evaluated using the binary-encounter-Bethe method with effective core potentials.[18]

The objective of the present study is to analyze low- and intermediate-energy electron interactions with titanium tetrachloride molecules. We report the results of measurements of total electron scattering cross section (TCS) from titanium tetrachloride molecules in low and intermediate energies. The results of theoretical calculations of elastic integral (ECS), differential (DCS), momentum transfer (MTCS), and ionization cross sections are also presented. This work is a continuation of our previous research on electron scattering from simple compounds with tetrahedral symmetry that are potential simple FEBID precursors of semiconducting and conducting layers, $X(CH_3)_4$ (X–C, Si, Ge)[20,21] and $SnCl_4$.[22,23]

II. EXPERIMENTAL

Experimental absolute TCS for the electron collisions with titanium tetrachloride molecules has been measured using the electrostatic electron spectrometer working in the linear transmission configuration under single collision conditions. As a detailed description of the applied method,[1] as well as the device[24] and procedures used,[25] was presented in our earlier works, only a brief summary is presented here.

The electron beam produced with an electron gun with thermionic filament is monoenergized ($\Delta E \simeq 80$ meV) in an energy dispersing cylindrical electrostatic 127° condenser and then is directed by an electrostatic lens system into a scattering cell, which is filled with the target vapor under study. The electrons leaving the collision chamber through the exit orifice in the forward direction are energetically discriminated with the retarding-field analyzer and finally are collected with the Faraday cup detector. The acceptance angle of the used electron detector system, defined by the lens apertures, is near 0.8 msr. The absolute total cross section, $Q(E)$, at each selected collision energy, E, is determined with the Beer–Lambert–Bouguer attenuation formula (BLB):

$$I_g(E) = I_0(E)\exp(-nLQ(E)),$$

where $I_g(E)$ and $I_0(E)$ are the intensities of the electron beam transmitted across the scattering cell measured with and without the target in the cell, respectively. L (=30.5 mm) is the path length of electrons in the reaction cell, while n denotes the number density of the target vapors determined from the measurements of the gas target pressure and temperatures of the scattering cell and manometer head. As the temperature of the cell (310–320 K) usually differs slightly from the temperature of the capacitance manometer head (kept at 322 K), the correction of gas target pressure reading due to the thermal transpiration effect[26,27] was taken into account. The TCS measurements have been carried out at different target-vapor pressures inside the scattering cell, which typically lay between 80 and 150 mPa. Under these conditions, no systematic variation of the measured TCSs with pressure is observed; thus, one can assume that multiple scattering events are not significant. The experimental absolute energy scale was calibrated against the well-known resonant oscillatory structure around 2.3 eV in molecular nitrogen,[28] while overall inaccuracy of the electron energy scale is estimated as about 0.1 eV. As a source of target $TiCl_4$ molecules, commercially available sample of declared purity better than 99.995% (Sigma-Aldrich) has been used.

The electrostatic electron spectrometer is maintained in a vacuum chamber with a background pressure of 10^{-5} Pa, obtained with the diffusion pump and a two-stage mechanical rotary pump system. The magnetic field in the electron optics and the reaction chamber is reduced by Helmholtz coils to the value below 0.1 μT. After opening/closing the leak valve, a relatively long delay was necessary to stabilize the target conditions in the scattering cell, which may generate some TCS uncertainty related to the target pressure determination.

The final TCS value at a given energy is an average of a large number of data measured in independent series (6–14) of individual runs (usually 10 in a series). Statistical uncertainties (one standard deviation of weighted mean values) are below 1% over the entire energy range studied. The direct sum of all potential individual systematic errors, related to determination of quantities necessary to TCS derivation, has been estimated to be up to 12% at the lowest energies applied, decreasing gradually to about 8% between 10 and 100 eV, and increasing to 10% at the highest collision energies that we operated. The reported data are not corrected for the forward-scattering effect (cf. Ref. 29). The quantities in the attenuation BLB formula are taken directly in the course of the experiment and, therefore, the TCS values reported in this work are given in absolute units, without any normalization procedure.

III. THEORETICAL AND COMPUTATIONAL METHODS

A. Low-energy elastic integral, differential, and momentum transfer cross section calculations: The Schwinger multichannel method

The Schwinger multichannel method (SMC)[30] is a variational approach used to obtain the scattering amplitude, and the present calculations were performed with the implementation that employs norm-conserving pseudopotentials,[31] in which the parameters of Bachelet, Hamann, and Schlüter (BHS)[32] were used to represent the nuclei and the core electrons in heavy atoms. This method has recently been revised,[33] and here, we focus on the discussion of the essential aspects concerning the present calculations. The scattering amplitude in the SMC method is written as[33]

$$f^{\mathrm{SMC}}(\vec{k}_f,\vec{k}_i) = -\frac{1}{2\pi}\sum_{m,n}\langle S_{\vec{k}_f}|V|\chi_m\rangle\left(d^{-1}\right)_{mn}\langle\chi_n|V|S_{\vec{k}_i}\rangle, \tag{1}$$

where

$$d_{mn} = \langle\chi_m|\frac{1}{2}(PV+VP) - VG_P^{(+)}V + \frac{\hat{H}}{N+1} - \frac{1}{2}\left(\hat{H}P+P\hat{H}\right)|\chi_n\rangle. \tag{2}$$

In the equations above, the $(N+1)$-electron trial bases of configuration-state functions (CSFs), $\{|\chi_m\rangle\}$, are given as products of target states with single-particle scattering orbitals with the proper spin-coupling and will be discussed in detail in the following paragraph. $|S_{\vec{k}_{i(f)}}\rangle$ is an eigenstate of the unperturbed Hamiltonian H_0, represented by the product of a target state and a plane wave with momentum $\vec{k}_{i(f)}$; V is the interaction potential between the incident electron and the electrons and nuclei of the target; $\hat{H} \equiv E - H$, where E is the collisional energy, and $H = H_0 + V$ is the scattering Hamiltonian; P is a projection operator onto the elastic channel, and $G_P^{(+)}$ is the free-particle Green's function projected on the P-space.

The calculations were performed in the static-exchange (SE) and static-exchange plus polarization (SEP) levels of approximations. The CSFs are constructed as

$$|\chi_{mn}\rangle = \mathcal{A}|\Phi_m^{(2s+1)}\rangle \otimes |\varphi_n\rangle, \tag{3}$$

where $\mathcal{A}$ is the antisymmetrization operator of $N+1$ electrons, $|\Phi_m^{(2s+1)}\rangle$ is a state of the molecular target, and $|\varphi_n\rangle$ is a scattering orbital. In the SE approximation, only the ground state of the molecular target $|\Phi_1^1\rangle$ $(m=1, s=0)$ described at the Hartree–Fock level is used to construct the CSFs. In the SEP approximation, the configuration space is enlarged and, in addition to the ground state, virtual, singly excited Slater determinants $|\Phi_m^{(2s+1)}\rangle$ $(m>1)$ representing the promotion of an electron from an occupied hole orbital to an unoccupied particle orbital with multiplicity $2s+1$ (1 for singlets and 3 for triplets) are also included in the construction of the CSFs. Only CSFs with $2s+1=2$ (doublets) are included in the expansion of the $(N+1)$-electron trial function.

We optimized the ground-state geometry of the target with the 6-31G(d) basis set at the Hartree–Fock level of theory, using the package GAMESS[34] in the T_d point group. With this, we obtained the value of 2.173 Å for the length of the Ti–Cl bond, which is close to the experimental value of 2.170 ± 0.002 Å.[8] In the scattering calculations, we employed the local-density norm-conserving pseudopotentials of BHS[32] to represent the nuclei core electrons of Ti and Cl atoms. In order to describe the valence electrons of titanium and chlorine atoms, we employed the Cartesian Gaussian (single-particle) basis using 5s5p5d for Ti (with exponents shown in Ref. 16) and 7s5p2d for Cl (with exponents shown in Ref. 23) atoms, which were generated using a variational method described in Ref. 35.

The scattering calculations were carried out within the C_{2v} group, since the SMC method deals only with Abelian groups. Whenever possible, the results were discussed in terms of the C_{2v} and T_d groups. Table I shows the correlations between these two point groups. In the SE approximation, we used the canonical Hartree–Fock orbitals. On the other hand, in the SEP approximation, we used improved virtual orbitals (IVOs)[36] to describe the particle and scattering orbitals [see Eq. (3)]. The IVOs were generated using the highest occupied molecular orbital of the a_1 symmetry as the hole orbital. The configuration space was constructed respecting the degeneracy of the T_d group, in such a way that in the SEP approximation, we use all 16 occupied orbitals as hole orbitals and the lowest 61 IVOs as particle and scattering orbitals. This proce-

TABLE I. Correlation table of T_d and C_{2v} point groups.

T_d	C_{2v}
A_1	A_1
T_1	$A_2 + B_1 + B_2$
T_2	$A_1 + B_1 + B_2$
E	$A_1 + A_2$
A_2	A_2

dure gave 15 531 CSFs for A_1, 14 924 for B_1 and B_2, and 14 327 for A_2 symmetries, providing a total of 59 706 configurations.

B. Low-energy elastic integral cross sections calculations: The R-matrix method

Scattering calculations were performed with UKRmol+ suite[37] with the R-matrix method, a detailed description of which can be found elsewhere.[38] The main concept of the R-matrix method lies in dividing the space into two areas: inner and outer region, separated by a sphere of a chosen radius a. In the inner region, N electrons of the target and the scattered electron are treated equally, taking into account exchange and correlation effects, under the assumption that one of the electrons is placed in the continuum or virtual orbital. The total scattering wavefunction is expanded with the basis functions ψ_k having the following form (following the standard notation[37]):

$$\psi_k = \mathcal{A}\sum_{ij} a_{ijk}\phi_i(x_1,\ldots,x_N)\gamma_j(x_{N+1}) + \sum_m b_{mk}\chi_m(x_1,\ldots,x_{N+1}), \quad (4)$$

called the close-coupling expansion. In this equation, $\mathcal{A}$ is the antisymmetrization operator, ϕ_i stands for the ith target state, γ_j refers to the continuum orbital of appropriate symmetry, and finally, χ_m denotes so-called L^2 functions. The ψ_k functions are imposed to be eigenvectors of the $N+1$ Hamiltonian, from which the expansion coefficients a_{ijk} and b_{mk} are obtained, as well as the R-matrix poles (E_k). Until this point, the calculations are independent of the scattering energy. The energy-dependent R-matrix can now be constructed from the basis functions and target states (cf. Refs. 37 and 38), and used in the outer region calculations. It is assumed that only one electron, placed in the single centered potential, can be found outside the sphere with radius $r = a$. The problems with the complexity of the target and exchange interactions are thus omitted. In the next steps, R-matrix is propagated[39] to a large radius $a_m \gg a$, and by matching to the asymptotic expansion of the outer-region radial function,[40] the K-matrix can be obtained. From simple algebraic relationships with S-matrix and T-matrix, other scattering quantities are readily computed.

Several models can be used for the description of the scattering process.[37] Two simple approaches can be applied for obtaining elastic cross sections, differing by the included χ_m functions from Eq. (4), namely, (1) static-exchange (SE) and (2) static-exchange with polarization (SEP) models, involving $N+1$-particle configurations of types

$$(\text{core})^{N-N_v}(\text{valence})^{N_v}(\text{continuum})^1, \quad (5)$$

$$(\text{core})^{N-N_v}(\text{valence})^{N_v}(\text{virtual})^1, \quad (6)$$

$$(\text{core})^{N-N_v}(\text{valence})^{N_v-1}(\text{virtual})^2, \quad (7)$$

where N_v is the number of valence electrons, and N is the total amount of the target electrons. The configurations in (6) and (7) represent possible shape resonances. The third configuration is actually used only in the SEP model, which we focus on in this work. The interpretation of cross sections has been preceded by the time-delay analysis, implemented in TIMEDELn[41] program. The time-delay matrix, or Q-matrix is expressed by the formula

$$\mathbf{Q}(E) = -i\hbar\mathbf{S}^*\frac{d\mathbf{S}}{dE}, \quad (8)$$

where $\mathbf{S}$ is the S-matrix. The largest eigenvalue of the Q-matrix corresponds to the longest time-delay of the scattering electron, q.[41] In the vicinity of the resonance, as a function of energy it can be described by a Lorentzian

$$q(E) = \frac{\hbar\Gamma}{(E-E_r)^2 + (\Gamma/2)^2} + bg(E), \quad (9)$$

where Γ is the resonance width, E_r is the resonance position on energy scale, and $bg(E)$ is the background contributions from other scattering processes. By fitting the appropriate Lorentzian, information about the position and width of the resonance can be obtained.

Target orbitals were obtained with the Hartree–Fock method in cc-pVDZ basis set. The optimization with MOLPRO[42–44] in this basis resulted in bond length $r(\text{Ti–Cl}) = 2.177$ Å, which is not so far from experimental value[8] 2.170 ± 0.002 Å. The first electron affinity determined experimentally is 2.88 eV,[11] whereas the vertical electron affinity (computed as the energy difference between the neutral molecule and anion, both in neutral geometry) obtained in our calculations is 4.09 eV. The valence electronic structure of the ground state and lowest-lying unoccupied orbitals is as follows:

$$(1a_1)^2(1t_2)^6(2a_1)^2(2t_2)^6(1e)^4(3t_2)^6(1t_1)^6, \quad (10)$$

$$(2e)(4t_2)(3a_1)(5t_2)(6t_2)(3e)(4a_1)(7t_2)(5a_1), \quad (11)$$

in T_d point group, in accordance with Nakatsuji *et al.*[45] However, the calculations with MOLPRO and UKRmol+ must have been performed in the C_{2v} group. The identification of T_d orbital symmetries was carried out with the use of the following relations introduced in Table I. All the single transitions from valence orbitals listed above in (10) were included in calculations. A total of 51 (19, 12, 12, and 8 of a_1, b_1, b_2, and a_2 symmetry, respectively) virtual orbitals (VOs) were used, giving 96 orbitals overall. The R-matrix radius was set to $18a_0$ so that the GTO basis could be applied, but it limited the possibilities of increasing the number of VOs included in calculations, as well as the use of diffuse functions. The exponents for the continuum GTOs were taken from Ref. 46 for $l \le 4$ and from Ref. 47 for $l = 5$. Calculations in quadruple precision with deletion thresholds set to 10^{-17} allowed keeping 99, 73, 73, and 48 continuum orbitals of a_1, b_1, b_2, and a_2 symmetry, respectively. In the free scattering mode, with such calculational setup, the eigenphase sums were below 10^{-3} rad, for collisional energies up to 9 eV. Radial charge densities were verified to be below 3×10^{-6} at the R-matrix radius in the cc-pVDZ basis set. The radius at which asymptotic expansion was applied was set to $100a_0$.

C. Ionization and intermediate energy elastic cross section calculations: The binary-encounter-Bethe and the additivity rule methods

To calculate electron -impact ionization cross section and elastic cross section for intermediate collisional energies, we have applied the binary-encounter-Bethe (BEB)[48] and additivity rule (AR)[49,50] methods, respectively.

Within BEB methods, the total cross section, σ^{Ion}, for the electron-induced ionization can be obtained as the sum of cross sections for ionization of each individual molecular orbital (MO)

$$\sigma^{\mathrm{Ion}} = \sum_{i=1}^{n_{\mathrm{MO}}} \sigma_i^{BEB}, \tag{12}$$

where n_{MO} is the number of given MOs. The electron-impact ionization cross section per individual MO orbital can be calculated according to the following formula:

$$\sigma^{BEB} = \frac{S}{t+u+1}\left[\frac{\ln t}{2}\left(1-\frac{1}{t^2}\right)+1-\frac{1}{t}-\frac{\ln t}{t+1}\right], \tag{13}$$

where $u = U/B$, $t = T/B$, $S = 4\pi a_0^2 N R^2/B^2$, $a_0 = 0.5292$ Å, $R = 13.61$ eV, and T is the electron impact energy. All molecular parameters, such as the electron binding energy, B, kinetic energy of the orbital, U, and orbital occupation number, N, have been calculated for the ground states of the geometrically optimized titanium tetrachloride molecules at the Hartree–Fock method level using the GAUSSIAN code,[51] and Gaussian 6-31++G basis set. Moreover, the ionization energies of the valence orbitals have been corrected using outer valence Green function calculations.[52]

According to the additivity rule (AR)[49,50] the total elastic cross section (ECS) can be calculated from cross sections for elastic electron scattering from constituent atoms of the target molecule.

To obtain the elastic electron-scattering cross sections for respective atoms, the radial Schrödinger equation

$$\left[\frac{\mathrm{d}^2}{\mathrm{d}r^2}-\frac{l(l+1)}{r^2}-2\left(V_{\mathrm{stat}}(r)+V_{\mathrm{polar}}(r)\right)+k^2\right]u_l(r)=0 \tag{14}$$

has been solved numerically with partial wave analysis. In calculations, the electron–atom interaction has been represented by static, $V_{\mathrm{stat}}(r)$,[53] and polarization, $V_{\mathrm{polar}}(r)$,[54] potentials.

IV. RESULTS AND DISCUSSION

The energy dependence of the present experimental absolute total cross section for electron scattering from $TiCl_4$ molecules is shown in Fig. 2. Numerical TCS data are listed in Table II. No experimental absolute electron-scattering TCS data for $TiCl_4$ molecules have been found in the literature for comparison. The positions of the resonances found experimentally and theoretically are summarized in Table III.

With respect to the magnitude, the measured TCS values for the $TiCl_4$ molecule are relatively high. Over the whole energy range investigated (0.3–300 eV), the TCS exceeds 18×10^{-20} m^2. Such high TCS is, at least in part, related to the large geometrical size of the $TiCl_4$ molecule; the gas kinetic cross section, σ_{gk}, for this molecular target (based on the van der Waals constant b[55]) amounts to 18.3×10^{-20} m^2.

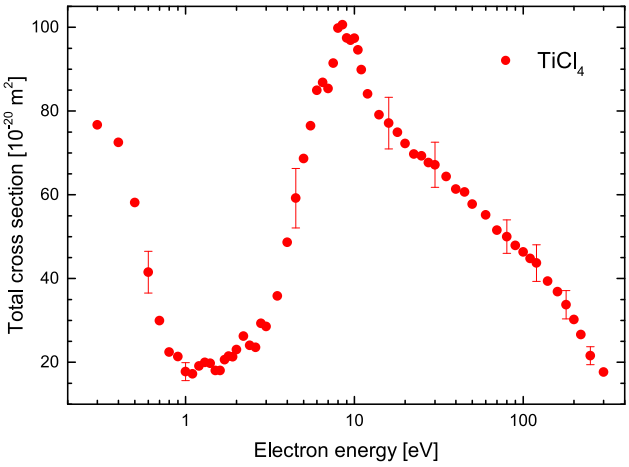

FIG. 2. Measured absolute total cross section for electron scattering from $TiCl_4$ molecules. Error bars shown at selected energies correspond to estimated overall experimental uncertainties.

According to the shape of the TCS energy curve, two very pronounced enhancements are visible, separated with the deep minimum located near 1.1 eV. Below this energy, TCS increases very sharply up to 76.7×10^{-20} m^2 at the lowest investigated energy,

TABLE II. Absolute experimental electron-scattering total cross sections (TCSs), at impact energy E (in eV), for the titanium tetrachloride ($TiCl_4$) molecule in units of 10^{-20} m^2.

E	TCS	E	TCS	E	TCS
0.3	76.7	3.0	28.6	22.5	69.7
0.4	72.5	3.5	35.8	25	69.3
0.5	58.1	4.0	48.6	27.5	67.7
0.6	41.5	4.5	59.2	30	67.2
0.7	30.0	5.0	68.6	35	64.4
0.8	22.4	5.5	76.5	40	61.3
0.9	21.3	6.0	85.0	45	60.7
1.0	17.8	6.5	86.8	50	57.8
1.1	17.3	7.0	85.4	60	55.2
1.2	19.1	7.5	91.5	70	51.5
1.3	20.0	8.0	99.8	80	50.0
1.4	19.8	8.5	101.0	90	47.9
1.5	18.0	9.0	97.4	100	46.3
1.6	18.0	9.5	96.9	110	44.8
1.7	20.6	10.0	97.4	120	43.7
1.8	21.5	10.5	94.6	140	39.4
1.9	21.3	11.0	89.9	160	36.8
2.0	23.0	12.0	84.1	180	33.8
2.2	26.3	14.0	79.1	200	30.2
2.4	24.0	16.0	77.1	220	26.6
2.6	23.6	18.0	74.9	250	21.6
2.8	29.3	20.0	72.3	300	17.7

TABLE III. Position of the resonances (in eV) found experimentally (Expt.) and theoretically (Theo.) through the R-matrix and SMC calculations in the SEP approximation and previously reported in the literature through a time-of-flight mass spectroscopy (ToFMS),[9] dissociative electron attachment (DEA),[10,14] and electron transmission spectroscopy (ETS)[15] experiments.

	Present			Kiser *et al.*[9]	Bennett *et al.*[10]	Bjarnason *et al.*[14]	Tossell *et al.*[15]	
Resonance	Expt.	Theo. TCS	Theo. R-matrix	Expt. SMC	Expt. ToFMS	Expt. DEA	Expt. DEA	ETS
T_2	4.8[a]	5.06	4.80	5.5	3.8	3.6	3.6	
A_1	6.5	6.3	6.30	6.5	5.7	5.3	5.8	
⋯	8.0[a]	⋯	⋯	⋯	⋯	⋯	8.2	
⋯	9.9	⋯	⋯	⋯	⋯	⋯	⋯	

[a]Evaluated due to detailed analysis of the main TCS maximum (see Fig. 7).

0.3 eV. Such strong increase toward thermal energies, which is not typical for non-polar targets (μ_D = 0D), can be related to the relatively large value of the static electric polarizability of the $TiCl_4$ molecule ($\alpha \approx 15.1 \times 10^{-30}$ m^3) and, hence, relatively strong induced polar interactions and also to the formation of a virtual state, which will be discussed latter. It is worth noting that the TCS curve clearly changes slope and becomes less steep below 0.4 eV. Above 1.5 eV, the TCS again increases and reaches its maximum value of about 101×10^{-20} m^2 close to 8.5 eV. Beyond the maximum TCS curve decreases with energy increase down to 18×10^{-20} m^2 at 300 eV, the upper limit of employed energy. On both sides of the main maximum, around 6.5 and 10 eV, two weak resonant-like features are visible. Two additional weak local maxima are discernible at around 1.3 and 2.2 eV, respectively. It is worth noting that the maxima at 6.5 and 10 eV were noticeable in each measurement series, while the other two discernible at around 1.3 and 2.2 eV, respectively, are somewhat statistical in nature. Due to the lack of detailed experimental data on individual scattering channels, the origin of the latter is rather unclear at the moment.

Strong and sharp changes in the TCS energy dependence can represent the resonant nature of scattering; however, detailed explanation of the resonant-like structures' origin is rather difficult without additional studies for particular scattering channels. In electron transmission studies of Tossell *et al.*, [15] broad structures were observed at around 3.6, 5.8, and 8.2 eV. It was also concluded by theoretical calculations that $TiCl_4$ with the addition of electron in the two lowest unoccupied orbitals ($2e$ and $4t_2$, following the standard enumeration, see also Sec. III B), form a stable anion, whereas two next orbitals ($3a_1$ and $5t_2$) may contribute to the near-threshold region of cross section. Thus, the rapid increase of TCS values toward the lowest measured energy can be partially assigned to the creation of metastable negative ion, $TiCl_4^-$. DEA studies of Bjarnason[14] showed the maxima of formation for $TiCl_3^-$ anion at 3.6 eV and Cl^- at 5.3 eV. By the analysis of the UV spectrum of $TiCl_4$, the first structure was attributed to a shape resonance of E symmetry or a Feshbach resonance of T_1 symmetry, and the second one was proposed to be the result of overlapping core-excited resonances. In the work of Bennett *et al.*,[10] the maxima of ion current after DEA were located at 3.8 and 5.7 eV and in studies of Kiser *et al.*[9] at 5.5 and 6.5 eV for $TiCl_3^-$ and Cl^-, respectively. Argumentation provided in (Bennett[10]) suggests that the lower energy process may involve species in their ground states, whereas in the second one, the remaining fragment ($TiCl_3$) must be in its excited state or other intermediate mechanisms occur. Calculations of cross sections for elastic scattering from $TiCl_4$ have been performed by Azevedo *et al.*,[16] showing a resonant-like structure around 6 eV and a large bump centered at 14 eV. Cross sections for electron impact ionization of $TiCl_4$ were also investigated both experimentally[13] and theoretically.[16] The measurements of electronic spectra in UV[56–58] revealed an electronic excitation threshold at around 4.4 eV, which was attributed to the $(1t_1 \rightarrow 2e)$ transition by SAC-CI calculations of Nakatsuji *et al.*[45]

Figure 3 shows elastic integral cross sections (ECSs) for $TiCl_4$ in the scattering symmetries of C_{2v} point group and the sum of them obtained using the R-matrix method within the SEP approximation. Since the symmetries b_1 and b_2 always occur in pairs in relations from Table I, these cross sections coincide. Below 7 eV, no clear, narrow resonance structures are observed. It was found that the R-matrix poles associated with configurations (g.s.) $\otimes$ $(2e)^1$ and (g.s.)

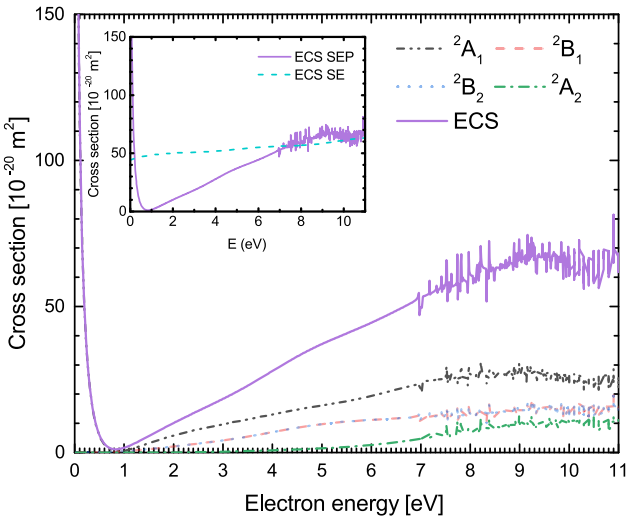

FIG. 3. Elastic cross sections (ECSs) obtained from the SEP approximation with the R-Matrix method; in particular, scattering symmetries and the sum of them. Inset shows the SE results for comparison.

$\otimes (4t_2)^1$ lay ~4 eV below the ground state of neutral target, showing that these two states should not be observed as shape resonances. This is also supported by the results in Ref. 15. The narrow peaks at around 7 eV and above that energy are likely to be pseudoresonances, which are structures with no physical meaning that appear in the ECS as a result of energetically accessible channels that are treated as closed in this level of approximation. The dominant configuration for the pole at 6.96 eV (exactly at the position of the first peak) corresponds to the first electronic transition ($1t_1 \rightarrow 2e$), with a scattering electron placed at $3a_1$ orbital. Below 7 eV, by detailed inspection of eigenvalues of the time-delay matrix (Fig. 4), two structures have been found that can be pre-attributed to broad and rather weak resonances. The one lower in energy occurs in $^2A_1$, $^2B_1$, and $^2B_2$ scattering symmetries of C_{2v} point group, which corresponds to the T_2 symmetry in T_d group. The result of Lorentzian fit by TIMEDELn located the resonance at E_r = 5.06 eV, having a very large width Γ = 4.49 eV. The biggest wavefunction coefficient for the closest pole common to A_1, B_1, and B_2 symmetries at 4.86 eV is 0.61, corresponding to the (g.s.) $\otimes (6t_2)^1$ state, while the others are less than 0.1. A small bump was also observed in the time-delay analysis in SE calculations (not shown). Therefore, this resonance may be off shape or mixed shape and core-excited type. The second structure was detected only in the A_1 symmetry at E_r = 6.3 eV, with a width Γ = 3 eV. The largest coefficient for the nearest pole is equal to 0.44 and corresponds to (g.s.) $\otimes$ $5a_1$ configuration, but $4a_1$ and higher orbitals of a_1 symmetry (in T_d point group) are not negligible. In SE calculations (time-delay not shown), where pseudoresonances are not observed, at least three resonant-like structures (one in A_1 and two in T_2 symmetry) were found around 8 eV; so, the A_1 resonance may also be of shape character, partially or fully.

In Fig. 5, the ECSs obtained from the SMC calculations are presented in the SEP and SE approximations, alongside the symmetry decomposition of the SEP ECS according to the C_{2v} point group. The overall behavior of the cross section is similar to the one obtained from the R-matrix calculation, where no distinct, sharp resonant structure can be seen. Yet, a small shoulder in the A_1, B_1, and B_2 symmetries in the SMC calculations can be observed around 4.5 eV, which may be associated with a shape resonance of the threefold-degenerate T_2 symmetry of the T_d point group. A minimum in the ECS can be seen around 1 eV and below this energy, the A_1 symmetry dominates the behavior of the cross section. The structures in higher impact energies are pseudoresonances. In the inset, the ECS calculated in the SE is presented and is in good agreement with the calculations performed by Azevedo *et al.*[16]

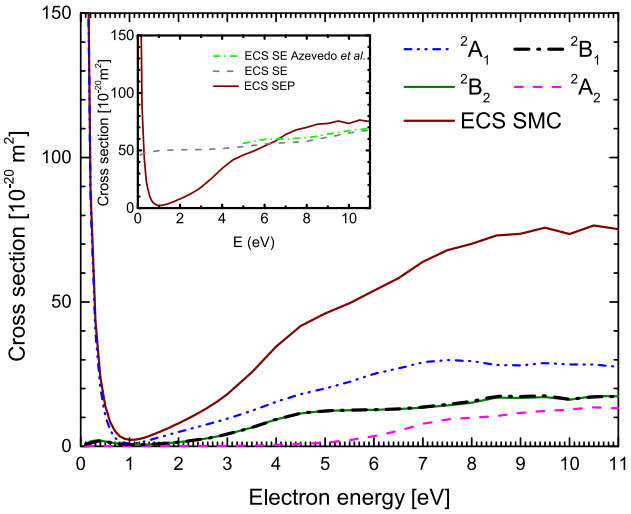

FIG. 5. Elastic integral cross sections obtained from the SEP approximation with the SMC method in the symmetries of the C_{2v} point group and the sum of them. The inset shows the SE results for comparison.

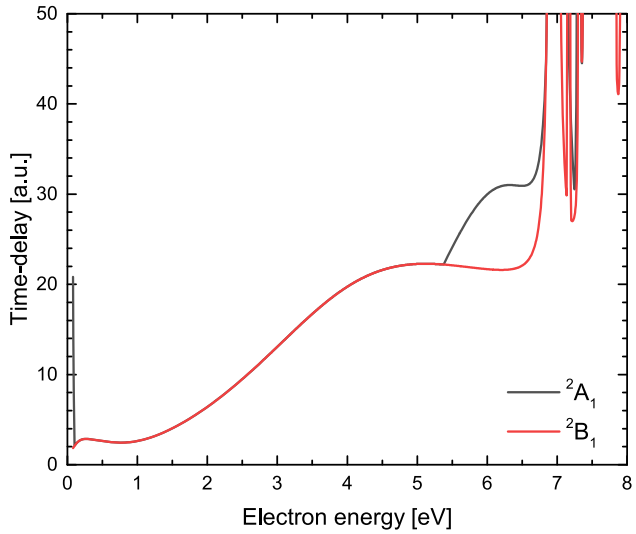

FIG. 4. The largest eigenvalue of the time-delay matrix obtained from the SEP approximation in $^2A_1$ and $^2B_1$ scattering symmetries.

From the diagonalization of the scattering Hamiltonian in the CSF basis set used in the SEP SMC calculations, we obtained that the lowest state of E and T_2 symmetries lay 4.83 and 4.18 eV below the ground state, respectively. These results corroborate the ones found by the present R-Matrix calculations, where two R-matrix poles also lay ~4 eV below the ground states, and are supported by the theoretical calculations of Tossell *et al.*[15] Beyond that, two resonant states were found. The first one at 4.80 eV in the A_1, B_1, and B_2 irreducible representations of the C_{2v} point group (T_2 symmetry of T_d) is associated with the first resonance found in the R-Matrix calculation (5.06 eV). It is worth noting that this resonance has the same symmetry and is close in energy to the small shoulder around 4.5 eV observed in the SMC cross section. Another resonant state of A_1 symmetry was found at 6.30 eV, corresponding to the second resonance found by the R-Matrix calculations (6.3 eV).

It should be emphasized that the theoretically obtained resonance structures are very weak and are barely observed in the calculated cross sections. The ETS features presented in the work of Tossell *et al.*[15] are also broad and are not strongly accentuated in the simulated cross section obtained from the derivative of transmitted current, although they appear lower in energy, as in other works on DEA of $TiCl_4$.[9,10,14] However, the described computational setup has many shortcomings, including a small number of virtual orbitals

and lack of diffuse functions in the basis set, whereas some of the orbitals included in calculations may be of Rydberg character.[45] Note that positions of resonances can be significantly shifted toward lower energies if diffusion functions are included in calculations. Another likely reason why the structures obtained are relatively weak and positioned at higher energies is their possible core-excited character. It is worth noting that the ECSs presented here greatly disagree with the one calculated by Tossell *et al.*[15] due to the different methods and approximations used in the calculations.

The comparison between the calculated ECSs and the measured TCSs is presented in Fig. 6. Although the theoretical cross sections agree well, they are lower than the experimental ones over the whole studied energy range. It is worth noting that the calculations are restricted to the elastic channel, while the measurements involve every accessible channel, including vibrational and rotational excitations, in addition to the elastic scattering. Therefore, the cross sections presented in Fig. 6 are not directly comparable. A sharp increase in the calculated SEP cross sections toward low energies in A_1 symmetry as well as in the TCS, is consistent with the presence of a virtual state. Besides, the minimum seen in both R-matrix and SMC SEP ECS, and in the TCS, is consistent with the presence of a Ramsauer–Townsend minimum. We argue that no low-energy resonance nor sharp increase toward 0 eV or minimum is observed in the SE approximation (see the insets in Figs. 3 and 5), since these two features depend on the proper description of polarization. Below 4 eV, the curve is not smooth, which could be partially explained by the existence of the lower structure appearing in the studies listed above around 3.6 eV. On the other hand, and attempt to approximate the TCS curve with the sum of Gaussian functions in the 4–12 eV energy range showed that four resonances may be observed, centered at around 4.8, 6.2, 8.0, and 9.9 eV, see Fig. 7. It is worth noting here that the *grand*-TCS, on the one hand, represents a sum of scattering information, and definitive assignments of broad features visible in the energy dependence of the TCS to particular scattering events are somehow uncertain. On the other hand, in TCS measurements, contrary to DEA experiments, all resonance signatures

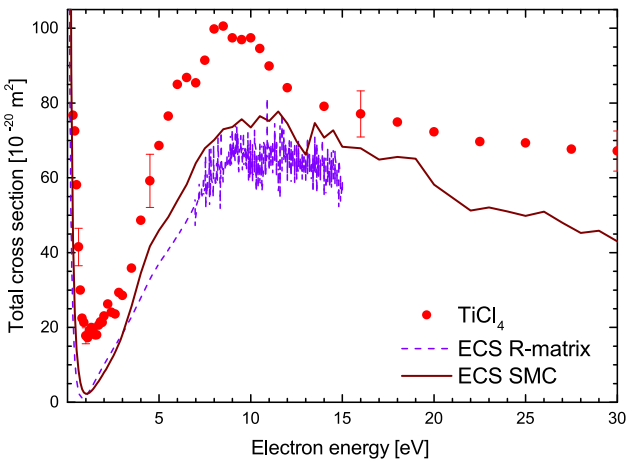

FIG. 6. Comparison of the experimental TCS with results of R-matrix (dashed violet line, ECS R-matrix) and SMC (full wine line, ECS SMC) calculations of the elastic integral cross section.

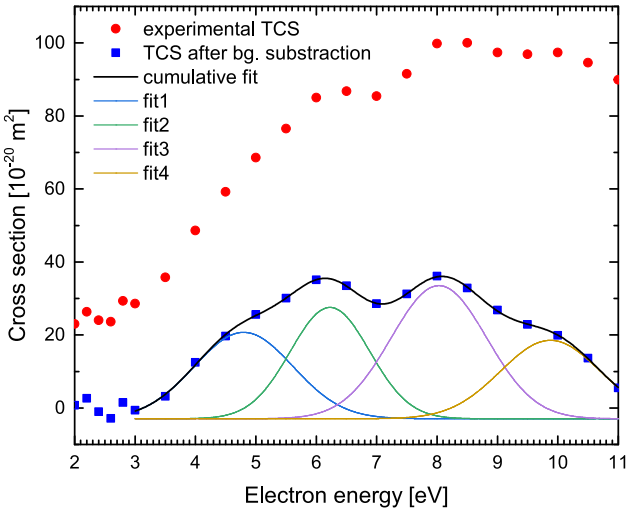

FIG. 7. Approximation of the TCS in 4–10 eV with four Gaussian curves, after the subtraction of the background scattering (assumed linear in this energy range).

will be present regardless of their decaying mechanisms.[59] Additionally, structures in TCS originating from the DEA process may be distorted or even obscured by contributions from other accessible processes, such as elastic scattering. When the resonance structures are broad, and the successive resonant states are close to each other, some weaker structures can also be partially masked by overlap with the low energy tail of the higher more intense resonance, resulting often in the shift of the energy position of a particular resonant structure. Moreover, the potential shift of the maximum in the DEA ion yield, as compared to the electron transmission spectroscopy (ETS) experiments, can be related to competition between autodetachment and dissociation in the relaxation of the initially formed transient negative ion. In the ETS spectrum, whole resonance width is reflected, and autodetachment will dominate over dissociation at higher energies. Thus, the DEA ion yield can be shifted to lower energies in comparison to the resonance positions observed in the ETS type experiments.[14] Since the DEA processes described above can be shifted toward higher energies in TCS, the structure at 4.8 eV may also correspond to the lower DEA process. For the reasons listed above, we think it is possible that it coincides with the weak resonance observed in ECS in T_2 symmetry at 5.06 and 4.80 eV, according to the R-matrix and SMC calculations, respectively. We used the fixed-nuclei approximation (FNA) in our calculations. In the FNA, the cross section is rotationally summed and vibrationally elastic. Up to 4 eV, the calculations fairly well reproduce the experimental curve qualitatively, and we believe that the quantitative differences are due to the lack of vibrational excitation channels in the calculations, since these inelastic cross sections may be of the order of 10 Å^2 (see, for instance, Christophorou *et al.*[60]). The lack of vibrational excitation cross sections in the literature for the $TiCl_4$ molecule makes it impossible to verify this hypothesis. A lack of polarization in the calculations of the cross sections of A_1 symmetry, responsible for the background of the Ramsauer–Townsend minimum, as shown in Fig. 8 (contribution of $l = 2$ partial wave), can also be playing a role in these differences. Unfortunately, improving

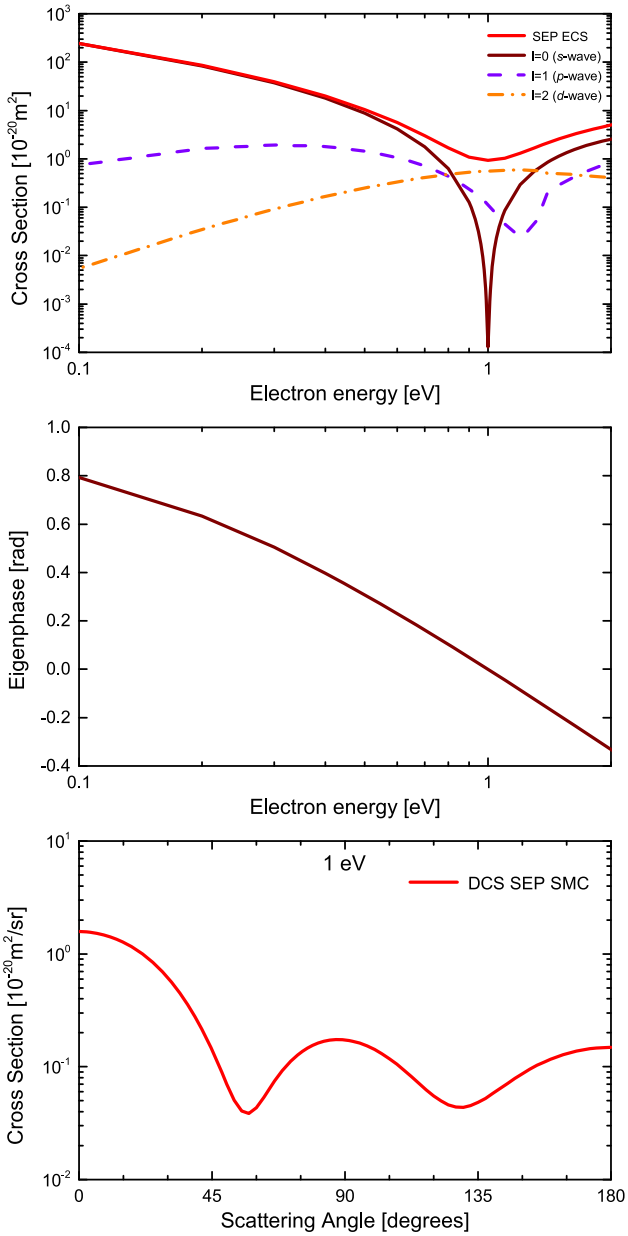

FIG. 8. Upper panel: Partial wave decomposition of the ECS: full red line, SEP ECS; full wine line, s-wave; dashed purple line, *p*-wave, and dashed-dotted orange line, *d*-wave. Middle panel: s-wave eigenphase. Lower panel: DCS SEP calculated with the SMC method at 1.0 eV. Both cross section and eigenphase support a virtual state and a Ramsauer–Townsend minimum.

the polarization scheme would be computationally unfeasible. The electronic excitation threshold[45] lies around 4.4 eV, which would explain the discrepancy between theory and experiment above this energy. It is reasonable to assume that the peak at 6.5 eV in the experimental TCS is moved toward higher energies due to the overlapping with higher resonances and electron-impact excitation processes (see Fig. 7). Therefore, we ascribe the 6.5 eV structure in TCS to the A_1 resonance at 6.3 eV in the theoretical R-matrix and SMC ECSs. Because it is much more pronounced in the TCS (in which, in general, resonances are blurred by inelastic processes), it is likely that this structure would be better described by calculations in which inelastic processes will be taken into account. Above 12 eV, the theoretical curves seem to follow the trend of experimental TCS, but due to the enormous amount of pseudoresonances, it is difficult to draw specific conclusions.

In order to investigate the SEP ECS behavior at the low energy regime in more detail, we plot in Fig. 8 the partial wave decomposition of the ECS, the s-wave eigenphase, and the differential cross section (DCS) at 1.0 eV, obtained from the SMC calculations. The s-wave results support the presence of a Ramsauer–Townsend minimum at around 0.99 eV, where the cross section goes to zero and the eigenphase changes sign, indicating that the effective potential felt by the electron, which is the combination of the attractive static polarization and the repulsive exchange interactions,[61–63] changes from attractive to repulsive. Although this minimum is observed, the ECS does not tend to zero around its position. This is a consequence of the *d*-wave ($l = 2$) contribution to the scattering process in this energy regime. In fact, both the partial wave decomposition and the DCS at 1.0 eV indicate that the electron–$TiCl_4$ interaction around this collisional energy is dominated by the *d*-wave scattering. We also observe a high magnitude in the s-wave cross section as the energy tends to zero. In polar molecules, the high magnitude in the low energy regime is due to the long-range dipole interactions between the target and the incident electron, while for non-polar molecules, such as $TiCl_4$, this sharp increase near zero energy may be associated with the formation of a virtual state. The virtual state is a resonance at zero energy, wherein the ideal case the cross section tends to infinity, the eigenphase tends to $\pi/2$, and the scattering length tends to negative infinity as the incident electron energy tends to zero. In the case of real molecules, a negative scattering length indicates the presence of the virtual state. Through the modified effective range theory (MERT)[64] we estimate the scattering length to be $-49.70a_0$ from the calculated SMC cross section, supporting the formation of a virtual state.

In Fig. 9, we present the DCSs calculated in both SE and SEP approximations for the impact energies of 3, 5, 10, 15, 20, and 30 eV obtained through the SMC method. The results in the SE approximation agree very well with the results from Azevedo *et al.*,[16] as expected. At 5 eV, the DCSs present a *d*-wave behavior. For the other energies, there is no dominant partial wave, indicating that distinct partial waves contribute to the scattering.

To complete the set of cross sections for the scattering of electrons by $TiCl_4$, in Fig. 10, the momentum transfer cross section (MTCS) calculated with the SMC is presented in the SE and SEP approximations. The dependence of the MTCS on impact energy is analogous to the ICS. Again, a good agreement between the present results in the SE approximation and the one from Azevedo *et al.*[16] is observed, as expected. The MTCS is a very important piece of information for plasma modelers, because of its relation to the transport of electrons in low-temperature plasma. For instance, the presence of a Ramsauer–Townsend minimum in the MTCS, as is the case for $TiCl_4$, favors the negative differential conductivity (NDC) effect. The NDC is the decrease of the electron drift velocity as a function of the density-reduced electric field $\mathcal{E}/N$ (where $\mathcal{E}$ is the electron field and

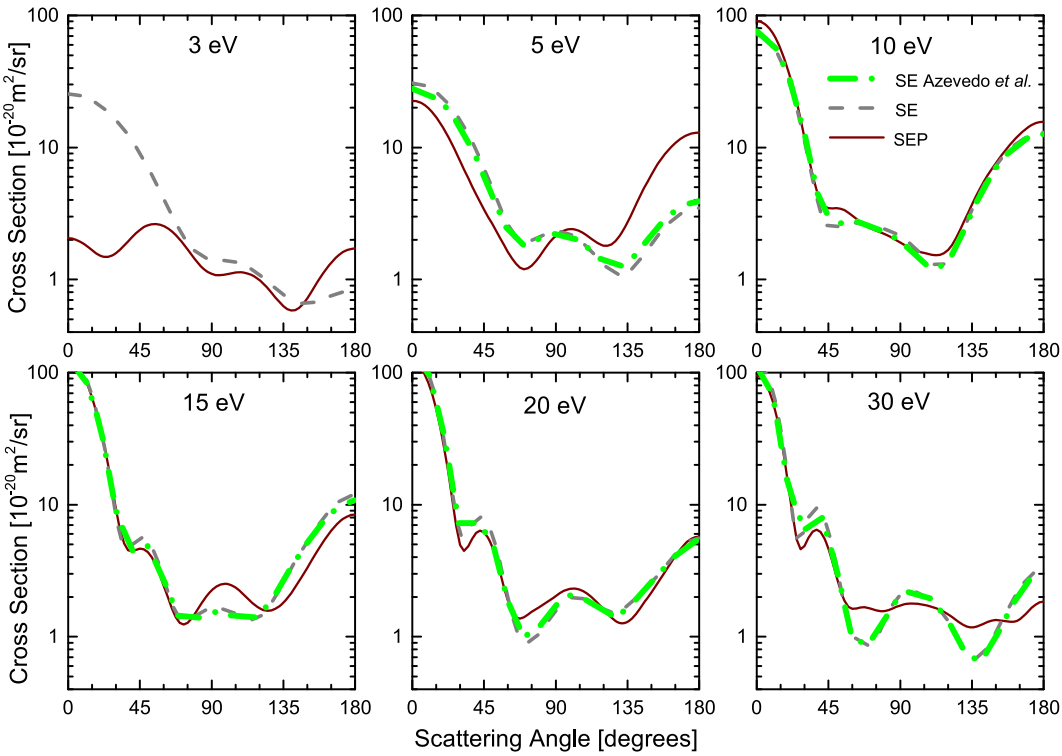

FIG. 9. Elastic differential cross sections for the scattering of electrons by $TiCl_4$ obtained through the SMC method. Dotted gray line, DCSs calculated in the SE approximation; full line, present SEP DCSs; dashed-dotted green line, SE DCSs from Azevedo *et al.*[16] A *d*-wave behavior is observed at 5 eV.

N is the neutral number density), as $\mathcal{E}$ increases[65] and can be avoided or enhanced depending on the application.[66]

Finally, in Fig. 11, experimental TCS values for intermediate electron energies are compared with integral (ECS) and total ionization (ICS) cross sections obtained using AR and BEB methods, respectively. The calculated threshold for ionization is 11.609 eV, and a maximum of 13.24×10^{-20} m^2 for the single ionization processes is predicted at 85 eV. Calculated ionization cross section is

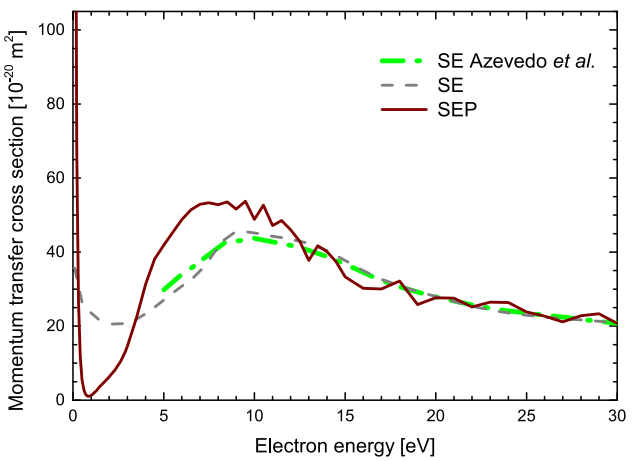

FIG. 10. Momentum-transfer cross section for the scattering of electrons by $TiCl_4$, obtained through the SMC method. Dotted gray line presents results in the SE approximation; full line presents SEP approximation; and long-dashed green line presents SE MTCS from the work of Azevedo *et al.*[16]

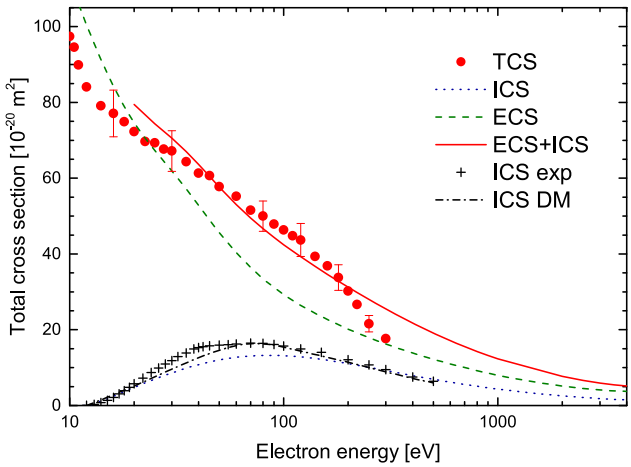

FIG. 11. Comparison of measured TCS with results of elastic (ECS) and ionization (ICS) cross section calculations at intermediate collisional energies. The sum of ECS and ICS (ICS + ECS), as well as experimental[13] (ICS exp) and theoretical[17] (ICS DM) total ionization cross sections are also shown for comparison.

in quite acceptable agreement with the experimental results,[13] but the ICS values are lower than experimental ones. In fact, the discrepancy between experimental and theoretical ICSs is mainly due to the fact that the results of the calculations take into account, in contrast to the experimental data, only single ionization processes. It is worth noting, that on one hand, the total ionization cross section calculated with the semiclassical DM formalism[17] is in much better agreement with experimental data than the results of our calculations. In addition, the value of the ionization cross section maximum (17.5×10^{-20} m^2) estimated using the BEB method with effective core potentials[18] is consistent with the experimental results. On the other hand, the present theoretical results are higher than those obtained previously[16] with the same method, but with a much more limited basis set [3-21G(3*d*)] used in the calculations of target electronic properties. From Fig. 11, it is clear that the elastic scattering predominates collisional processes above 30 eV. Below 25 eV, calculated ECS is too high and even exceeds the TCS, which is associated with limitations of the AR model used in the computations.

To estimate the TCS for electron scattering from the $TiCl_4$ molecule at high impact energies, which lay beyond the upper accessible limit, in our experiment we have used the sum of calculated ECS and ICS. While, due to limitations of the methods used in the calculations, such approximation is rather simple and rough, it has been shown that it can lead to satisfactory results.[67] For collisional energies between 30 and 200 eV, the sum of ECS and ICS is close to the measured TCS values. Above 200 eV, the experimental TCS values are clearly below the data from the theoretical estimations, which shows, on the one hand, the limitations of this approach, and on the other hand, it may indicate that TCS measured for the highest energies can be somewhat underestimated due to not sufficient discrimination of electrons scattered inelastically into the forward direction.

V. CONCLUSIONS

Measured TCS for the scattering of electrons by $TiCl_4$ was reported in the 0.3–300 eV energy range. The TCS is large for near-threshold collisional energies, it presents a minimum at around 1.5 eV, and resonant structures around 6.5, 8.5, and 10 eV. An attempt to approximate the TCS in the 4–10 eV with Gaussian curves showed that 4 resonances centered around 4.8, 6.2, 8.0, and 9.9 eV may be present in the scattering process. Calculated ECS, DCS, MTCS, and total ionization cross sections for $TiCl_4$ were also reported with different levels of theory. A good qualitative agreement was found between the calculated ECSs and the measured TCSs below 4 eV. Although no distinct, sharp resonant structure is observed in the calculated ECSs, the R-matrix and SMC calculations at the SEP level of approximation showed two weak resonances, one centered around 4.8 eV of T_2 symmetry and another around 6.3 eV of A_1 symmetry. Below 1 eV, both the experimental TCSs and calculated ECSs show a large increase as the collisional energy decreases. Investigations of the very low-energy s-wave cross section and eigenphase obtained with the SMC SEP calculation support a Ramsauer–Townsend minimum near 1 eV and the formation of a virtual state at the lowest impact energies. Diagonalization of the scattering Hamiltonian of the SMC SEP calculations and analysis of the R-matrix poles showed that the two lowest scattering states lie below the ground state. While the cross sections reported here form a good and reliable dataset, further work regarding other scattering channels, such as the electronic excitation channels, is needed to provide a complete set of electron–$TiCl_4$ cross section for plasma modelers.

ACKNOWLEDGMENTS

This work was supported, in part, by the Polish Ministry of Science and Education (Grant No. MNiE Project 2022-2023). Numerical calculations have been performed at the Academic Computer Center (TASK) in Gdańsk. This work was also supported by the Brazilian agencies Conselho Nacional de Desenvolvimento Científico e Tecnológico (CNPq) and Coordenação de Aperfeiçoamento de Pessoal de Nível Superior (CAPES). P.A.S.R., G.M.M., and M.H.F.B. acknowledge computational support from Professor Carlos Alberto Martins de Carvalho at LFTC-DFIS-UFPR and at LCPAD-UFPR. N.T. and P.M. would also like to thank Dr. Jimena Gorfinkiel for the valuable substantive discussion and significant assistance in handling the UKRmol+ program.

AUTHOR DECLARATIONS

Conflict of Interest

The authors have no conflicts to disclose.

Author Contributions

Natalia Tańska: Data curation (equal); Formal analysis (equal); Investigation (equal); Methodology (equal); Software (equal); Validation (equal); Visualization (equal); Writing – original draft (equal). **Pedro A. S. Randi**: Data curation (equal); Formal analysis (equal); Investigation (equal); Methodology (equal); Software (equal); Validation (equal); Visualization (equal); Writing – original draft (equal). **Sylwia Stefanowska-Tur**: Data curation (equal); Formal analysis (equal); Investigation (equal); Methodology (equal); Validation (equal); Visualization (equal); Writing – original draft (equal). **Giseli M. Moreira**: Data curation (equal); Formal analysis (equal); Investigation (equal); Methodology (equal); Software (equal); Validation (equal); Visualization (equal); Writing – original draft (equal). **Elżbieta Ptasińska-Denga**: Data curation (equal); Formal analysis (equal); Investigation (equal); Methodology (equal); Validation (equal); Visualization (equal); Writing – original draft (equal). **Márcio H. F. Bettega**: Conceptualization (equal); Data curation (equal); Formal analysis (equal); Investigation (equal); Methodology (equal); Resources (equal); Software (equal); Supervision (equal); Validation (equal); Visualization (equal); Writing – original draft (equal). **Czesław Szmytkowski**: Data curation (equal); Formal analysis (equal); Investigation (equal); Methodology (equal); Resources (equal); Supervision (equal); Validation (equal); Visualization (equal); Writing – original draft (equal). **Paweł Możejko**: Conceptualization (equal); Data curation (equal); Formal analysis (equal); Investigation (equal); Methodology (equal); Resources (equal); Supervision (equal); Validation (equal); Visualization (equal); Writing – original draft (equal).

DATA AVAILABILITY

The data that support the findings of this study are available within the article.

REFERENCES

[1] C. Szmytkowski and P. Możejko, Eur. Phys. J. D **74**, 90 (2020).
[2] J. Patscheider, L. Shizhi, and S. Vepřek, Plasma Chem. Plasma Process. **16**, 341 (1996).
[3] S. H. Kim and G. A. Somorjai, J. Phys. Chem. B **106**, 1386 (2002).
[4] Y. Ohshita and K. Watanabe, J. Cryst. Growth **203**, 540–546 (1999).
[5] D. Hössler and M. Ernst, Solid State Electron. **158**, 51–58 (2019).
[6] L. O. Brockway and F. T. Wall, J. Am. Chem. Soc. **56**, 2373 (1934).
[7] M. W. Lister and L. E. Sutton, Trans. Faraday. Soc. **37**, 393 (1941).
[8] Y. Morino and H. Uehara, J. Chem. Phys. **45**, 4543 (1966).
[9] R. W. Kiser, J. G. Dillard, and D. L. Dugger, Adv. Chem. **72**, 153 (1968).
[10] S. L. Bennett, R. E. Pabst, J. L. Margrave, and J. L. Franklin, Int. J. Mass Spectrom. Ion Phys. **15**, 451 (1974).
[11] B. P. Mathur, E. W. Rothe, and G. P. Reck, Int. J. Mass Spectrom. Ion Phys. **31**, 77 (1979).
[12] R. G. Egdell and A. F. Orchard, J. Chem. Soc., Faraday Trans. 2 **74**, 485 (1978).
[13] R. Basner, M. Schmidt, K. Becker, V. Tarnovsky, and H. Deutsch, Thin Solid Films **374**, 291 (2000).
[14] E. H. Bjarnason, B. Ómarsson, S. Engmann, F. H. Ómarsson, and O. Ingólfsson, Eur. Phys. J. D **68**, 121 (2014).
[15] J. A. Tossell, J. H. Moore, and J. K. Olthoff, J. Phys. B: At. Mol. Phys. **20**, 565 (1987).
[16] D. L. Azevedo, M. H. F. Bettega, L. G. Ferreira, and M. A. P. Lima, J. Phys. B: At., Mol. Opt. Phys. **33**, 5467 (2000).
[17] H. Deutsch, K. Becker, S. Matt, and T. D. Märk, Int. J. Mass Spectrom. **197**, 37 (2000).
[18] G. E. Scott and K. K. Irikura, Surf. Interface Anal. **37**, 973 (2005).
[19] B. M. Bode and M. S. Gordon, J. Mol. Graphics Modell. **16**, 133 (1998).
[20] S. Stefanowska-Tur, P. Możejko, E. Ptasińska-Denga, and C. Szmytkowski, J. Chem. Phys. **150**, 094303 (2019).
[21] P. A. S. Randi, G. M. Moreira, and M. H. F. Bettega, Phys. Rev. A **102**, 022812 (2020).
[22] P. Możejko, S. Stefanowska-Tur, E. Ptasińska-Denga, and Cz. Szmytkowski, J. Chem. Phys. **151**, 064305 (2019).
[23] P. A. S. Randi and M. H. F. Bettega, J. Appl. Phys. **127**, 233301 (2020).
[24] C. Szmytkowski and P. Możejko, Vacuum **63**, 549 (2001).
[25] C. Szmytkowski, P. Mozejko, and G. Kasperski, J. Phys. B: At., Mol. Opt. Phys. **31**, 3917 (1998).
[26] M. Knudsen, Ann. Phys. **336**, 205 (1910).
[27] K. F. Poulter, M.-J. Rodgers, P. J. Nash, T. J. Thompson, and M. P. Perkin, Vacuum **33**, 311 (1983).
[28] C. Szmytkowski, K. Maciag, and G. Karwasz, Phys. Scr. **54**, 271 (1996).
[29] M. J. Brunger, S. J. Buckman, and K. Ratnavelu, J. Phys. Chem. Ref. Data **46**, 023102 (2017).
[30] K. Takatsuka and V. McKoy, Phys. Rev. A **24**, 2473 (1981); *ibid.* **30**, 1734 (1984).
[31] M. H. F. Bettega, L. G. Ferreira, and M. A. P. Lima, Phys. Rev. A **47**, 1111 (1993).
[32] G. B. Bachelet, D. R. Hamann, and M. Schlüter, Phys. Rev. B **26**, 4199 (1982).
[33] R. F. da Costa, M. T. d. N. Varella, M. H. F. Bettega, and M. A. P. Lima, Eur. Phys. J. D **69**, 159 (2015).
[34] G. M. J. Barca, C. Bertoni, L. Carrington, D. Datta, N. De Silva, J. E. Deustua, D. G. Fedorov, J. R. Gour, A. O. Gunina, E. Guidez, T. Harville, S. Irle, J. Ivanic, K. Kowalski, S. S. Leang, H. Li, W. Li, J. J. Lutz, I. Magoulas, J. Mato, V. Mironov, H. Nakata, B. Q. Pham, P. Piecuch, D. Poole, S. R. Pruitt, A. P. Rendell, L. B. Roskop, K. Ruedenberg, T. Sattasathuchana, M. W. Schmidt, J. Shen, L. Slipchenko, M. Sosonkina, V. Sundriyal, A. Tiwari, J. L. Galvez Vallejo, B. Westheimer, M. Włoch, P. Xu, F. Zahariev, and M. S. Gordon, J. Chem. Phys. **152**, 154102 (2020).
[35] M. H. F. Bettega, A. P. P. Natalense, M. A. P. Lima, and L. G. Ferreira, Int. J. Quantum Chem. **60**, 821 (1996).
[36] W. J. Hunt and W. A. Goddard III, Chem. Phys. Lett. **3**, 414 (1969).
[37] Z. Mašín, J. Benda, J. D. Gorfinkiel, A. G. Harvey, and J. Tennyson, Comput. Phys. Commun. **249**, 107092 (2020).
[38] J. Tennyson, Phys. Rep. **491**, 29 (2010).
[39] L. A. Morgan, Comput. Phys. Commun. **31**, 419 (1984).
[40] C. J. Noble and R. K. Nesbet, Comput. Phys. Commun. **33**, 399 (1984).
[41] D. A. Little, J. Tennyson, M. Plummer, C. J. Noble, and A. G. Sunderland, Comput. Phys. Commun. **215**, 137 (2017).
[42] MOLPRO, version 2020.1, a package of *ab initio* programs, H. J. Werner, P. J. Knowles, G. Knizia, F. R. Manby, M. Schütz, P. Celani, W. Györffy, D. Kats, T. Korona, R. Lindh, A. Mitrushenkov, G. Rauhut, K. R. Shamasundar, T. B. Adler, R. D. Amos, S. J. Bennie, A. Bernhardsson, A. Berning, D. L. Cooper, M. J. O. Deegan, A. J. Dobbyn, F. Eckert, E. Goll, C. Hampel, A. Hesselmann, G. Hetzer, T. Hrenar, G. Jansen, C. Köppl, S. J. R. Lee, Y. Liu, A. W. Lloyd, Q. Ma, R. A. Mata, A. J. May, S. J. McNicholas, W. Meyer, T. F. Miller III, M. E. Mura, A. Nicklass, D. P. O'Neill, P. Palmieri, D. Peng, K. Pflüger, R. Pitzer, M. Reiher, T. Shiozaki, H. Stoll,A. J. Stone, R. Tarroni, T. Thorsteinsson, M. Wang, and M. Welborn, see https://www.molpro.net.
[43] H.-J. Werner, P. J. Knowles, G. Knizia, F. R. Manby, and M. Schütz, Wiley Interdiscip. Rev.: Comput. Mol. Sci. **2**, 242 (2012).
[44] H.-J. Werner, P. J. Knowles, F. R. Manby, J. A. Black, K. Doll, A. Heßelmann, D. Kats, A. Köhn, T. Korona, D. A. Kreplin, Q. Ma, T. F. Miller, A. Mitrushchenkov III, K. A. Peterson, I. Polyak, G. Rauhut, M. Sibaev, and M. Sibaev, J. Chem. Phys. **152**, 144107 (2020).
[45] H. Nakatsuji, M. Ehara, M. H. Palmer, and M. F. Guest, J. Chem. Phys. **97**, 2561 (1992).
[46] M. Tarana and J. Tennyson, J. Phys. B: At., Mol. Opt. Phys. **41**, 205204 (2008).
[47] A. Loupas and J. D. Gorfinkiel, J. Chem. Phys. **150**, 064307 (2019).
[48] W. Hwang, Y. K. Kim, and M. E. Rudd, J. Chem. Phys. **104**, 2956 (1996).
[49] D. Raj, Phys. Lett. A **160**, 571 (1991).
[50] K. N. Joshipura and P. M. Patel, Z. Phys. D **29**, 269 (1994).
[51] M. J. Frisch, G. W. Trucks, H. B. Schlegel, G. E. Scuseria, M. A. Robb, J. R. Cheeseman, G. Scalmani, V. Barone, B. Mennucci, G. A. Petersson, H. Nakatsuji, M. Caricato, X. Li, H. P. Hratchian, A. F. Izmaylov, J. Bloino, G. Zheng, J. L. Sonnenberg, M. Hada, M. Ehara, K. Toyota, R. Fukuda, J. Hasegawa, M. Ishida, T. Nakajima, Y. Honda, O. Kitao, H. Nakai, T. Vreven, J. A. Montgomery, Jr., J. E. Peralta, F. Ogliaro, M. Bearpark, J. J. Heyd, E. Brothers, K. N. Kudin, V. N. Staroverov, T. Keith, R. Kobayashi, J. Normand, K. Raghavachari, A. Rendell, J. C. Burant, S. S. Iyengar, J. Tomasi, M. Cossi, N. Rega, J. M. Millam, M. Klene, J. E. Knox, J. B. Cross, V. Bakken, C. Adamo, J. Jaramillo, R. Gomperts, R. E. Stratmann, O. Yazyev, A. J. Austin, R. Cammi, C. Pomelli, J. W. Ochterski, R. L. Martin, K. Morokuma, V. G. Zakrzewski, G. A. Voth, P. Salvador, J. J. Dannenberg, S. Dapprich, A. D. Daniels, O. Farkas, J. B. Foresman, J. V. Ortiz, J. Cioslowski, and D. J. Fox, Gaussian 09, Revision D.01 (Gaussian, Inc., Wallingford, CT, 2009).
[52] V. G. Zakrzewski and W. von Niessen, J. Comput. Chem. **14**, 13 (1994).
[53] F. Salvat, J. D. Martinez, R. Mayol, and J. Parellada, Phys. Rev. A **36**, 467 (1987).
[54] N. T. Padial and D. W. Norcross, Phys. Rev. A **29**, 1742 (1984).
[55] *Handbook of Chemistry and Physics*, 76th ed., edited by D. R. Lide (CRC Press, Boca Raton, 1995–1996).
[56] A. A. Iverson and B. R. Russell, Spectrochim. Acta, Part A **29**, 715 (1973).
[57] C. Dijkgraaf, Spectrochim. Acta **21**, 769 (1965).
[58] C. A. L. Becker, C. J. Ballhausen, and I. Trabjerg, Theor. Chim. Acta **13**, 355 (1969).
[59] A. I. Lozano, F. Kossoski, F. Blanco, P. Limão-Vieira, M. T. d. N. Varella, and G. Garcia, J. Phys. Chem. Lett. **13**, 7001 (2022).
[60] L. G. Christophorou, J. K. Olthoff, and M. V. V. S. Rao, J. Phys. Chem. Ref. Data **25**, 1341 (1996).
[61] M. A. P. Lima, K. Watari, and V. McKoy, Phys. Rev. A **39**, 4312 (1989).
[62] B. H. Lengsfield III, T. N. Rescigno, and C. W. McCurdy, Phys. Rev. A **44**, 4296 (1991).
[63] B. M. Nestmann, K. Pfingst, and S. D. Peyerimhoff, J. Phys. B: At., Mol. Opt. Phys. **27**, 2297 (1994).
[64] K. Fedus, G. P. Karwasz, and Z. Idziaszek, Phys. Rev. A **88**, 012704 (2013).
[65] N. A. Dyatko, I. V. Kochetov, and A. P. Napartovich, Plasma Sources Sci. Technol. **23**, 043001 (2014).
[66] G. Schaefer and K. H. Schoenbach, IEEE Trans. Plasma Sci. **14**, 561 (1986).
[67] C. Szmytkowski, S. Stefanowska, M. Zawadzki, E. Ptasińska-Denga, and P. Możejko, Phys. Rev. A **94**, 042706 (2016).